



# Effects of temperature on factors relevant to laser operation near 1.6 $\mu\text{m}$ wavelength in resonantly (in-band) pumped $\text{CaF}_2\text{:Er}$ and $\text{SrF}_2\text{:Er}$ crystals: a comparative study

R. Lisiecki<sup>1</sup> · B. Macalik<sup>1</sup> · J. Komar<sup>1</sup> · R. Kowalski<sup>1</sup> · A. Strzep<sup>1,2</sup> · Zhen Zhang<sup>2</sup> · Zhonghan Zhang<sup>2</sup> · Yunfei Wang<sup>2</sup> · Liangbi Su<sup>2</sup> · W. Ryba-Romanowski<sup>1</sup>

Received: 19 June 2023 / Accepted: 21 July 2023 / Published online: 27 July 2023  
© The Author(s) 2023

## Abstract

Single crystals of  $\text{CaF}_2$  and  $\text{SrF}_2$  containing  $\text{Er}^{3+}$  ions with concentrations between 0.01 and 0.6 at% respectively, were grown using the temperature gradient technique (TGT). Absorption spectra related to the  $^4\text{I}_{15/2} \rightarrow ^4\text{I}_{13/2}$  transition of  $\text{Er}^{3+}$  ions were measured at 5 K to investigate the properties of the crystal field splitting of the  $^4\text{I}_{13/2}$  multiplet, and at several temperatures in the region 80 K – 300 K to determine the effect of temperature on the spectral bands. The  $^4\text{I}_{13/2} \rightarrow ^4\text{I}_{15/2}$  luminescence spectra were recorded within the same temperature range as for absorption measurement. The analysis of absorption and luminescence spectra provides an in-depth knowledge on the effect of temperature on the factors that govern the efficiency of resonant optical pumping near 1.6  $\mu\text{m}$  and the resulting lasing ability of  $\text{Er}^{3+}$  ions imbedded in  $\text{CaF}_2$  and  $\text{SrF}_2$  hosts.

## 1 Introduction

Laser action near 1.6  $\mu\text{m}$  in  $\text{CaF}_2\text{:Er}^{3+}$  has been reported for the first time by S.A. Pollack in 1963 [1]. In this study a cylindrical rod of  $\text{CaF}_2$  doped with 0.1 mol% of  $\text{Er}^{3+}$  ions was 2 inches in length and 3/8 inches in cross section. It was pumped with a filtered radiation of a xenon flashlamp that delivered light pulses with an input energy of about 1000 J. The measured quantum efficiency of the  $^4\text{I}_{13/2} \rightarrow ^4\text{I}_{15/2}$  laser transition excited by pumping into the 375 nm absorption band was about 2% at room temperature and about 6–7% near 77 K. The observed laser performance was not encouraging and for a long time this system has been discarded as laser active material. In subsequent years a considerable interest was paid to the investigation of the structural and optical properties of rare earth doped  $\text{BaF}_2$ ,  $\text{CaF}_2$  and  $\text{SrF}_2$  hosts in order to understand the nature of luminescent sites and the activator-activator and activator-host interaction.

Gathered knowledge combined with observed peculiarities of laser performance of  $\text{Er}^{3+}$  ions in other fluoride hosts such as  $\text{LiYF}_4$  [2], or  $\text{BaY}_2\text{F}_8$  [3] made it possible to discover a new laser potential of  $\text{CaF}_2$ , and  $\text{SrF}_2$  hosts heavily doped with  $\text{Er}^{3+}$  ions.

Indeed, C. Labbe et al. [4] reported laser performance of heavily doped  $\text{Er}^{3+}\text{:CaF}_2$  under various pump wavelengths. The laser emitted at 2.8  $\mu\text{m}$  upon pumping at 970 nm with a threshold absorbed pump power of 23 mW and slope efficiency of 30%. It is worth noticing that the pumping wavelength of 970 nm is advantageous in that the upper laser level  $^4\text{I}_{11/2}$  is populated directly assuring thereby the highest pumping efficiency. The authors also observed the laser operation under pumping at 800 or 1545 nm but with a smaller efficiency. In virtually all hosts the lifetime of initial level for the  $^4\text{I}_{11/2} \rightarrow ^4\text{I}_{13/2}$  laser transition of  $\text{Er}^{3+}$  ions is shorter than that of the terminal laser level and the laser emission at 2.8  $\mu\text{m}$  is self-terminated. At high concentration of  $\text{Er}^{3+}$  ions the ion-ion interaction and nonlinear excitation mechanisms are able to overcome this obstacle, however. T.T. Basiev et al. [5] reported CW laser operation in  $\text{Er}^{3+}(5\%)\text{:CaF}_2$  and  $\text{Er}^{3+}(5\%)\text{:SrF}_2$  crystals near 2.75  $\mu\text{m}$  with output power of 0.4 and 2 W respectively, upon transverse pumping with a diode laser at 980 nm. Continuous tuning of laser wavelength between 2720 and 2760 nm was achieved in  $\text{Er}^{3+}(5\%)\text{:SrF}_2$  crystal. The bulk thermal damage thresholds measured for

✉ R. Lisiecki  
r.lisiecki@intibs.pl

<sup>1</sup> Institute of Low Temperature and Structure Research, Polish Academy of Sciences, Okólna 2, 50-422 Wrocław, Poland

<sup>2</sup> Key Laboratory of Transparent and Opto-Functional Inorganic Materials, Shanghai Institute of Ceramics, Chinese Academy of Sciences, 215 Chengbei Road, Shanghai 201800, China

$\text{Er}^{3+}(5\%):\text{CaF}_2$  and  $\text{Er}^{3+}(5%):\text{SrF}_2$  crystals were approximately the same and equal to  $500 \text{ W cm}^{-3}$ . These reports have been followed by numerous papers devoted mainly to laser operation near  $2.75 \mu\text{m}$  in  $\text{Er}^{3+}:\text{CaF}_2$  with different concentration of  $\text{Er}^{3+}$  ions. For instance, J. Sulc et al. [6] reported on  $\text{Er}^{3+}:\text{CaF}_2$  ceramic  $2.79 \mu\text{m}$  tunable laser, Ma et al. [7] investigated the effect of  $\text{Er}^{3+}$  concentration on laser performance of  $\text{Er}^{3+}:\text{CaF}_2$  crystals, Ma et al. [8] reported on improved CW laser performance from a diode-pumped  $\text{Er,Pr}:\text{CaF}_2$  crystal. Mingqui Fan et al. [9] reported on  $2.79 \mu\text{m}$  CW laser operation with a slope efficiency of 41%. Zhen Zhang et al. and Yunfei Wang et al. achieved efficient  $\sim 2.8 \mu\text{m}$  CW lasers in extremely lightly doped  $\text{Er}:\text{CaF}_2$  crystals with concentration of 0.5 at.% and 0.3 at.% [10, 11].

The experimental data related to laser operation near  $2.8 \mu\text{m}$  in  $\text{Er}^{3+}:\text{CaF}_2$  and  $\text{Er}^{3+}:\text{SrF}_2$  are abundant and the interplay between linear and nonlinear processes governing the  ${}^4\text{I}_{11/2} \leftrightarrow {}^4\text{I}_{13/2}$  transitions involved is understood. Instead, the knowledge of spectroscopic features relevant to the  ${}^4\text{I}_{13/2} \rightarrow {}^4\text{I}_{15/2}$  laser transition of  $\text{Er}^{3+}$  near  $1.6 \mu\text{m}$  in calcium and strontium fluoride is very poor. A paper by Kumar et al. [12] was devoted to this issue. Some related information is included in papers by Labbe [13] and R. Svecar et al. [14] devoted essentially to laser operation near  $2.8 \mu\text{m}$ . On the other hand the  ${}^4\text{I}_{13/2} \rightarrow {}^4\text{I}_{15/2}$  laser operation of  $\text{Er}^{3+}$  near  $1.6 \mu\text{m}$  under direct pumping into the upper laser level has been observed in other erbium-doped hosts. Ter-Gabrielyan et al. investigated the effect of pump wavelength on laser performance of cryo-cooled  $\text{Er}^{3+}:\text{YAG}$  laser [15]. Nemeč et al. reported laser performance of tunable resonantly pumped  $\text{Er}:\text{GGAG}$  laser [16]. Ter-Gabrielyan et al.

compared spectroscopic and laser properties of resonantly (in-band) pumped  $\text{Er}:\text{YVO}_4$  and  $\text{Er}:\text{GdVO}_4$  crystals [17].

In the present work we explore the effect of temperature on optical spectra of absorption and emission transitions between the  ${}^4\text{I}_{15/2}$  and  ${}^4\text{I}_{13/2}$  multiplets of  $\text{Er}^{3+}$  ions imbedded in  $\text{CaF}_2$  and  $\text{SrF}_2$  crystals. The aim of the work is to interpret the thermally induced change of contribution of transitions involved based on in-depth analysis of observed spectra and determine the spectroscopic parameters relevant to resonant optical pumping of the  ${}^4\text{I}_{13/2}$  upper laser level and the  ${}^4\text{I}_{13/2} \rightarrow {}^4\text{I}_{15/2}$  laser operation at 300 K and at cryogenic temperatures down to 80 K. To the best of our knowledge, these issues have not been reported before.

## 2 Experimental

The  $\text{Er}^{3+}:\text{CaF}_2$  and  $\text{Er}^{3+}:\text{SrF}_2$  crystals were grown in Shanghai Institute of Ceramics, Chinese Academy of Sciences using the temperature gradient technique (TGT). The detailed growth process is described in [18]. The purity of the  $\text{Er}^{3+}:\text{CaF}_2$  and  $\text{Er}^{3+}:\text{SrF}_2$  crystals was examined with a powder X-ray diffraction method using a Siemens D5000 diffractometer equipped with a copper radiation tube. The measurements were performed in a  $2\theta$  angle range of  $5\text{--}90^\circ$  with a  $0.04^\circ$  step and a count-time of 4 s/step. The XRD patterns are presented in Fig. 1. The appeared doublet lines are related to the unfiltered  $\text{K}\alpha_1$  and  $\text{K}\alpha_2$  characteristic Cu X-ray radiation. The selected physicochemical properties of  $\text{CaF}_2$  and  $\text{SrF}_2$  crystals are listed in Table 1. An Agilent Cary 5000 spectrophotometer was used to record unpolarized absorption spectra as

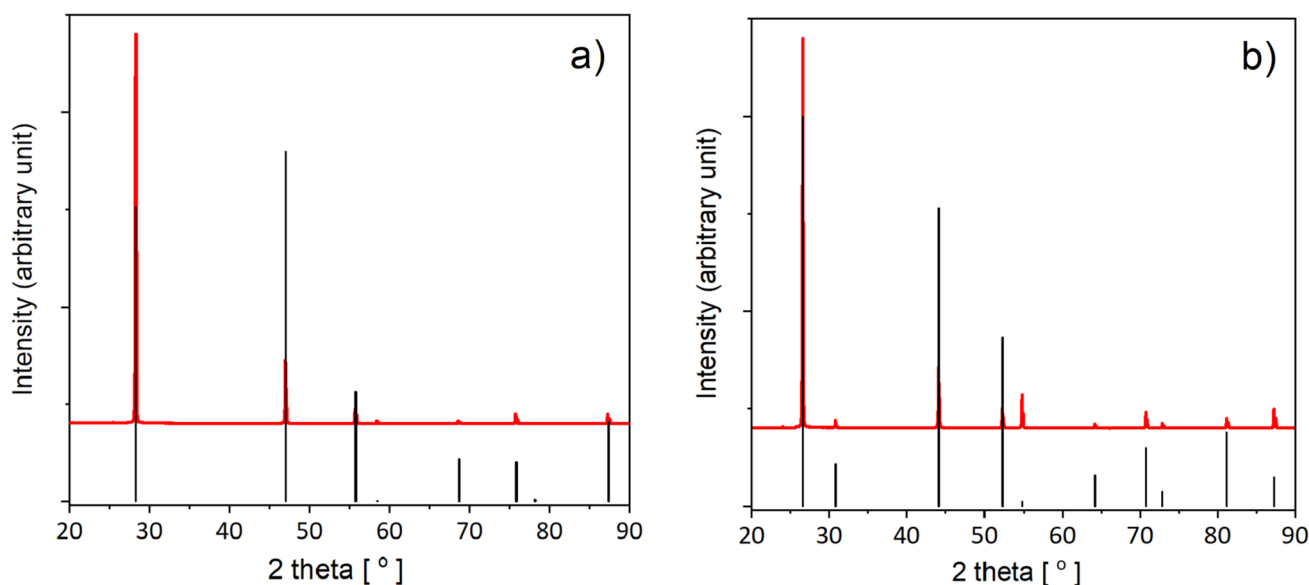


**Fig. 1** XRD patterns of **a**  $\text{CaF}_2$  and **b**  $\text{SrF}_2$  crystals (red) and the referenced patterns taken from the ICSD database (black)

**Table 1** Selected physicochemical properties of  $\text{CaF}_2$  and  $\text{SrF}_2$  crystals

	$\text{CaF}_2$	$\text{SrF}_2$
Crystal structure	Fm $\bar{3}$ m (225)-cubic $a=5.4629 \text{ \AA}$ , $V=163.03 \text{ \AA}^3$ , $Z=4$	Fm $\bar{3}$ m (225)-cubic $a=5.800 \text{ \AA}$ , $V=195.11 \text{ \AA}^3$ , $Z=4$
Density [ $\text{g}/\text{cm}^3$ ]	3.18	4.29
Thermal Conductivity [ $\text{W}/\text{m}\cdot\text{K}$ ]	9.71	8.30
Refractive index	1.43	1.44
First order Raman vibration [ $\text{cm}^{-1}$ ]	322 [19]	285 [20]
Energy gap [eV]	12.10	11.25

a function of 5 K-300 K temperature. Absorption spectra were measured with an instrumental bandwidth set to 0.05 nm. Near infrared emission spectra were excited by a 975 nm CNI diode laser, dispersed by an Optron DongWoo monochromator with 750 mm focal length and detected by an InGaAs detector. A xenon lamp 380 nm and Hamamatsu R-3896 photomultiplier were used to record the visible luminescence. During temperature-dependent experiments,  $\text{Er}^{3+}:\text{CaF}_2$  and  $\text{Er}^{3+}:\text{SrF}_2$  crystals were mounted in an Oxford Instruments continuous flow liquid helium cryostat equipped with a temperature controller.

### 3 Results and discussion

Several factors are responsible for the effects of temperature on absorption and emission spectra. First of all, thermal line broadening (1), a mechanism consisting of Raman scattering of phonons by an ion in an excited state (2) and thermal line shift which determines the change of transition energy due to temperature induced displacement of levels (3) involved in the transitions. As result, these factors affect the populations of both the initial and the terminal levels.

In the  $4f^{11}$  configuration of  $\text{Er}^{3+}$  ions the lowest energy multiplets are the  $^4I_{15/2}$  ground state and the  $^4I_{13/2}$  first excited state. They are separated by about  $6500 \text{ cm}^{-1}$ . When  $\text{Er}^{3+}$  ions are incorporated in a crystal host the crystal field splits the ground multiplet and the excited multiplet into a number of crystal field sublevels. In addition, the disparity of size and/or valency between incorporated erbium ions and substituted cations in the crystal structure creates sites differing in the symmetry and strength of the crystal fields. This feature is related to the systems considered in this study.

Figure 2 shows the room temperature absorption spectra of the  $^4I_{15/2} \rightarrow ^4I_{13/2}$  transition for several concentrations of  $\text{Er}^{3+}$  ions in  $\text{CaF}_2$  and  $\text{SrF}_2$  crystals. The spectra consist of a broad band extending from 1400 to 1650 nm, where several peaks can be identified. Some structures on their tops may be discerned. In these structures the most prominent local peaks are located at 1506, 1517, 1528, 1530 and 1543 nm

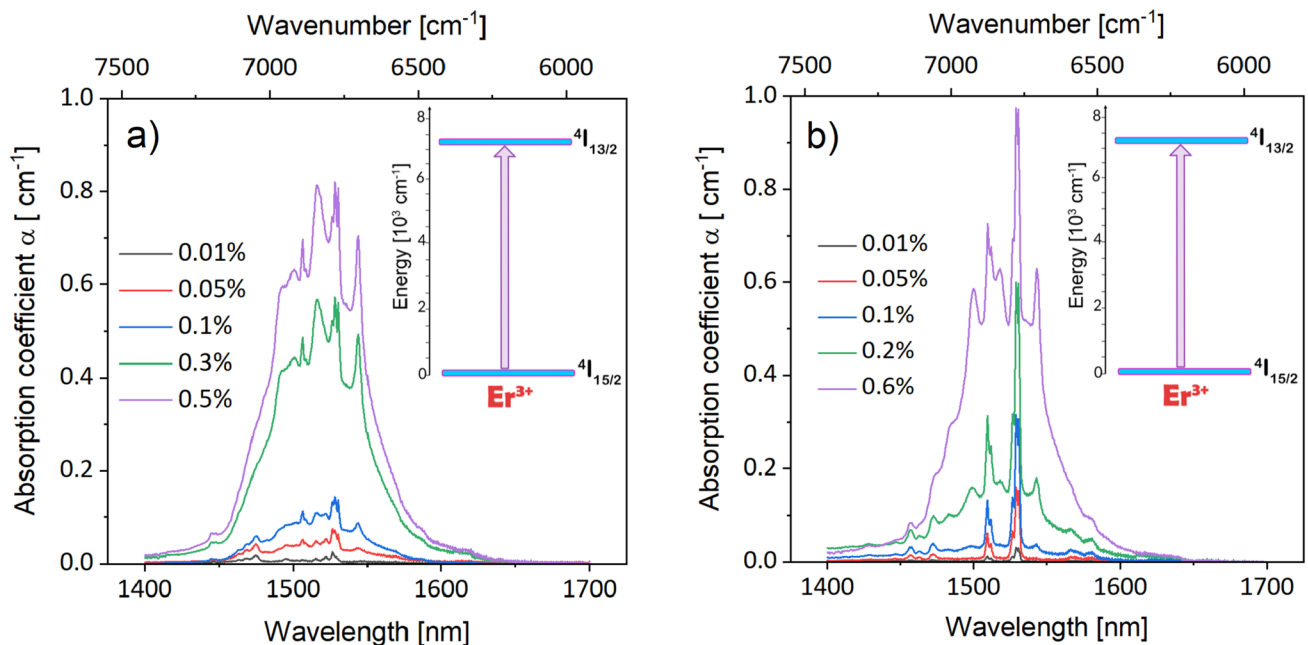


**Fig. 2** Room temperature absorption spectra of the  $^4I_{15/2} - ^4I_{13/2}$  transition measured for several concentrations of  $\text{Er}^{3+}$  ions in **a**  $\text{CaF}_2$  and **b**  $\text{SrF}_2$  crystals. Insets show an involved  $\text{Er}^{3+}$  energy levels scheme

for Er<sup>3+</sup> in CaF<sub>2</sub> and at 1499, 1510, 1529, 1530 and 1543 nm for Er<sup>3+</sup> in SrF<sub>2</sub>.

It is worth noticing that the shapes of bands recorded at different concentrations of Er<sup>3+</sup> in CaF<sub>2</sub> crystal show some differences. The same concerns the spectra for Er<sup>3+</sup> ions in SrF<sub>2</sub> crystal.

The optimal Er<sup>3+</sup> concentration in an active medium with a resonantly pumped <sup>4</sup>I<sub>13/2</sub> → <sup>4</sup>I<sub>15/2</sub> laser transition usually stems from a trade-off between endeavor to minimize an adverse self-absorption effect and to maintain sufficient pumping efficiency. It can be seen in Fig. 2 that the peak value of absorption coefficient for a CaF<sub>2</sub> crystal containing 0.5at% Er<sup>3+</sup> (1.22 × 10<sup>20</sup> ion/cm<sup>3</sup>) and a SrF<sub>2</sub> crystal containing 0.6at% Er<sup>3+</sup> (1.23 × 10<sup>20</sup> ion/cm<sup>3</sup>) equals to 0.82 cm<sup>-1</sup> and 0.98 cm<sup>-1</sup> respectively.

From the spectra presented in Fig. 2, it follows for example that an end-pumped 1 cm in length cylindrical rod will absorb 56% (Er:CaF<sub>2</sub>) and 62% (Er:SrF<sub>2</sub>) of the incident light (1528 nm) power, respectively. Therefore, in the rest of this paper, we will limit our discussion to the 0.5at% Er:CaF<sub>2</sub> and 0.6at% Er:SrF<sub>2</sub>.

Experimental oscillator strengths *P<sub>exp</sub>* of the <sup>4</sup>I<sub>15/2</sub> → <sup>4</sup>I<sub>13/2</sub> absorption transition were evaluated using relation [21]:

$$P_{exp} = \frac{mc}{\pi e^2 N} \int \alpha(\nu) d\nu \tag{1}$$

In this expression, *m* is the electron mass, *e* is the electron charge, *N* is the Er<sup>3+</sup> concentration, *ν* is the frequency and *α(ν)* is the absorption coefficient expressed in cm<sup>-1</sup>.

The integrals *fα(ν)dν* correspond to the absorption bands and the resulting *P<sub>exp</sub>* values are 2.27 × 10<sup>-6</sup> and 1.85 × 10<sup>-6</sup> for Er<sup>3+</sup>:CaF<sub>2</sub> and Er<sup>3+</sup>:SrF<sub>2</sub>, respectively. The experimental oscillator strength *P<sub>exp</sub>* = 2.2 × 10<sup>-6</sup> of the <sup>4</sup>I<sub>15/2</sub> → <sup>4</sup>I<sub>13/2</sub> absorption transition of Er<sup>3+</sup> in CaF<sub>2</sub> reported by Kumar et al. [12] is consistent with our finding. It is worth noticing that the Er<sup>3+</sup> concentration in a sample investigated in [12] is likely to be markedly smaller. The authors inconsistently state that Er concentration in the studied sample is 0.01 wt% and 0.01 at% in abstract of their article [12]. Peak absorption coefficient of 0.17 cm<sup>-1</sup> then reported [12] is smaller by a factor of 5, roughly than that measured for CaF<sub>2</sub> doped with 0.5at% Er<sup>3+</sup> mentioned above.

When incorporating trivalent rare earth ion into CaF<sub>2</sub> or SrF<sub>2</sub> lattice the incorporated ion substitutes divalent Ca<sup>2+</sup> or Sr<sup>2+</sup> cation and the disparity of charge should be compensated. Different ways of charge compensation are possible, for instance co-doping with H<sup>+</sup> ions [22], D<sup>+</sup> ions [23], Na<sup>+</sup> ions [24] or by incorporated F<sup>-</sup> ions. Varieties of optical centers created by different ways are markedly different, however. In our samples the charge compensation is made by F<sup>-</sup> ions located in the interstitial sites. It is commonly agreed that for a low doping level the luminescent

centers consist of a single Er<sup>3+</sup> ion located in three possible sites: the tetragonal sites where the F<sup>-</sup> is in the nearest neighbor interstitial site, the trigonal sites where the F<sup>-</sup> is in the second nearest neighbor interstitial site and the cubic sites when F<sup>-</sup> is far from the Er<sup>3+</sup> ion. When the Er<sup>3+</sup> concentration increases the dimer, trimer and more complex clusters showing completely dissimilar natures are formed. The onset of cluster creation is not a stepwise phenomenon. Consequently, the limit of a low doping level mentioned above is not obvious. Tallant and Wright [25] investigated CaF<sub>2</sub> crystal samples containing 0.01 mol% and 0.2 mol% of Er<sup>3+</sup> employing a high resolution site selective spectroscopy. They concluded that the onset of clustering occurs already at 0.05 mol% concentration and it may be predominant at 0.3 mol% concentration. Brown et al. [26] investigated SrF<sub>2</sub> crystals doped with Er<sup>3+</sup> ions with concentration ranged from 0 to 1% using electron spin resonance technique. The authors observed variation of tetragonal and trigonal sites and concluded that this can be explained by a calculation of relative energies of interstitial fluorine ions.

Figure 3 compares the <sup>4</sup>I<sub>15/2</sub> → <sup>4</sup>I<sub>13/2</sub> absorption spectra recorded for Er<sup>3+</sup>:CaF<sub>2</sub> and Er<sup>3+</sup>:SrF<sub>2</sub> samples at 5 K. The spectrum for Er<sup>3+</sup>:SrF<sub>2</sub> is inverted for the sake of clarity. We assign a line at 1536 nm in the Er<sup>3+</sup>:CaF<sub>2</sub> spectrum to transition between the lowest crystal field component of the ground multiplet and the lowest crystal field component at energy 6512 cm<sup>-1</sup> of the <sup>4</sup>I<sub>13/2</sub> multiplet (the 0–0 line). Similarly, we assign a line at 1540 nm (6496 cm<sup>-1</sup>) as 0–0 line for

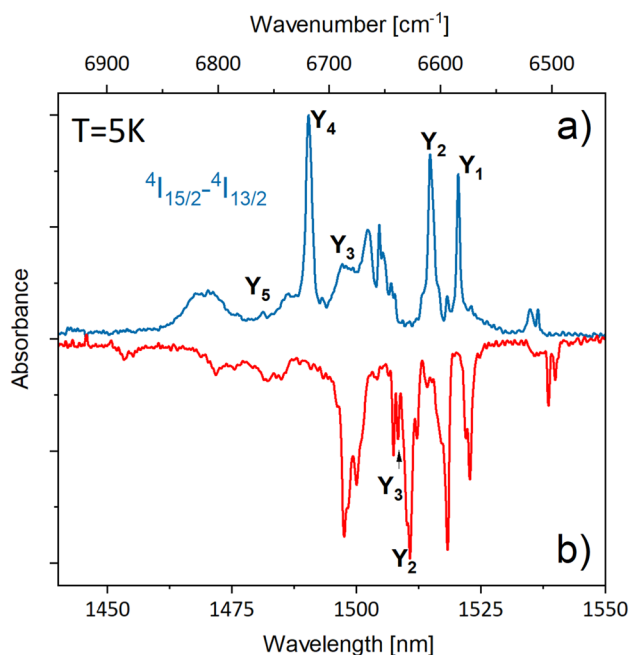


Fig. 3 The <sup>4</sup>I<sub>15/2</sub>–<sup>4</sup>I<sub>13/2</sub> absorption spectra recorded for a Er:CaF<sub>2</sub> and b Er:SrF<sub>2</sub> samples at 5 K. Spectrum for Er:SrF<sub>2</sub> is inverted for the sake of clarity. See text for explaining meanings of Y<sub>i</sub> symbols

Er<sup>3+</sup>:SrF<sub>2</sub> sample. The spectra extend to about 1450 nm and consist of numerous components with the most prominent at 1490, 1514 and 1520 nm for Er<sup>3+</sup> in CaF<sub>2</sub> and at 1497, 1510, 1518 and 1523 nm for Er<sup>3+</sup>:SrF<sub>2</sub>. To understand spectral distribution of the observed bands we refer to results of extensive investigation performed in the past employing methods of EPR, site selective spectroscopy, optical Zeeman spectroscopy and infrared spectroscopy. Rector et al. [27] reported a study of EPR and optical Zeeman spectra of CaF<sub>2</sub> crystal containing 0.1 mol% Er<sup>3+</sup> ions. The EPR spectra disclosed the existence of cubic, tetragonal and trigonal sites in the approximate ratios 15:20:1 whereas the optical spectrum consisted predominantly of lines due to tetragonal sites. The authors determined energies of 6 tetragonal (C<sub>4v</sub>) CF levels of the <sup>4</sup>I<sub>13/2</sub> multiplet. Five of them: 6572.9, 6602, 6684.7, 6716.8, 6747.2 cm<sup>-1</sup> coincide with lines indicated by Y<sub>1</sub>–Y<sub>5</sub> in Fig. 3. Wells et al. [28] reported on polarized selective excitation studies of the C<sub>3v</sub> symmetry centers in BaF<sub>2</sub> and SrF<sub>2</sub> doped with Er<sup>3+</sup>. The authors determined energies of 6 trigonal (C<sub>3v</sub>) CF levels of the <sup>4</sup>I<sub>13/2</sub> multiplet for Er<sup>3+</sup> in SrF<sub>2</sub>. Two of them: 6622 and 6634 cm<sup>-1</sup> coincide with lines indicated by Y<sub>2</sub> and Y<sub>3</sub> in Fig. 3. Spectral lines due to cubic sites of rare earth ions in CaF<sub>2</sub> and SrF<sub>2</sub> have been also observed, for example, weakly luminescent transitions of Sm<sup>3+</sup> in CaF<sub>2</sub> and SrF<sub>2</sub> have been assigned to centers of cubic symmetry [29]. More recently [24] luminescence of Nd<sup>3+</sup> optical centers close to cubic symmetry in CaF<sub>2</sub> was observed, albeit their intensity was weak. The <sup>4</sup>I<sub>15/2</sub> ↔ <sup>4</sup>I<sub>13/2</sub> magnetic dipole transitions are allowed therefore absorption and emission intensities of Er<sup>3+</sup> in cubic sites may be higher. B. Jeżowska-Trzebiatowska et al. [30] investigated low temperature magnetic susceptibility, infrared and Raman spectra of Cs<sub>2</sub>ErCl<sub>6</sub> single crystal in which Er<sup>3+</sup> ions are located solely in sites of O<sub>h</sub> symmetry. The authors found that the <sup>4</sup>I<sub>15/2</sub> → <sup>4</sup>I<sub>13/2</sub> absorption spectrum at 5 K consists of predominant lines of magnetic dipole transitions ending on 5 CF levels of the <sup>4</sup>I<sub>13/2</sub> state and markedly weaker vibronic lines induced by odd normal vibrations of the ErCl<sub>6</sub><sup>3-</sup> moiety. The oscillator strength P<sub>exp</sub> = 0.33 × 10<sup>-6</sup> has been determined subsequently [31] for the <sup>4</sup>I<sub>15/2</sub> → <sup>4</sup>I<sub>13/2</sub> transition. These findings indicate that the contribution of magnetic dipole transition is small and our values of oscillator strength for Er<sup>3+</sup>:CaF<sub>2</sub> and Er<sup>3+</sup>:SrF<sub>2</sub> are due mainly to electric dipole transitions in tetragonal and trigonal centers.

Based on the low temperature <sup>4</sup>I<sub>13/2</sub> → <sup>4</sup>I<sub>15/2</sub> and <sup>4</sup>S<sub>3/2</sub> → <sup>4</sup>I<sub>15/2</sub> emission spectra, it was found that overall <sup>4</sup>I<sub>15/2</sub> ground state splitting is about 500 cm<sup>-1</sup> and 450 cm<sup>-1</sup> for Er<sup>3+</sup>:CaF<sub>2</sub> and Er<sup>3+</sup>:SrF<sub>2</sub>, respectively. However, the several trigonal CF levels have been located above 496 cm<sup>-1</sup> in Er<sup>3+</sup>:SrF<sub>2</sub> [28]. It is worth noticing that details of the ground state splitting provided by luminescence and EPR spectroscopy are supplemented by far

infrared spectroscopy. In fact, Aubry et al. [32] investigated absorption spectra in the region 17–170 cm<sup>-1</sup> and Zeeman effect at 1.4 K for SrF<sub>2</sub> crystal containing rare earth ions with concentration of 0.2 mol%. They attributed lines observed at 32.8 and 43.5 cm<sup>-1</sup> to electronic transition of Er<sup>3+</sup> ions in tetragonal site (C<sub>4v</sub>) and a line at 81.3 cm<sup>-1</sup> to electronic transition of Er<sup>3+</sup> ions in cubic site (O<sub>h</sub>).

Figure 4 compares absorption spectra (upper) and emission spectra (medium) at several different temperatures between 80 and 300 K for Er<sup>3+</sup>:CaF<sub>2</sub> crystal. Graphs in the bottom are plots of the gain coefficient G(λ) evaluated according to the relation [33]:

$$G(\lambda) = N[P\sigma_e(\lambda) - (1 - P)\sigma_a(\lambda)] \quad (2)$$

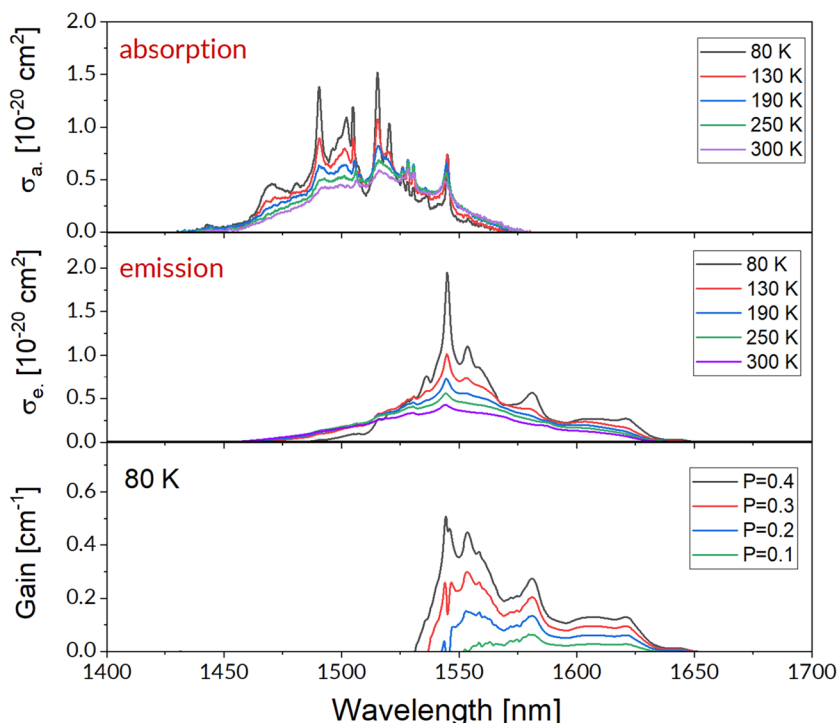
where,  $N$  is Er<sup>3+</sup> ions concentration,  $P$  denotes a population inversion parameter defined as the ratio of erbium ions density in the excited state to the overall erbium ion density in the crystal,  $\sigma_e(\lambda)$  is the stimulated-emission cross-section and  $\sigma_a(\lambda)$  is the absorption cross-section.

To compare absorption ability of samples differing in chemical composition and/or density of absorbing ions the absorption spectrum is expressed in cross-section units. Five temperatures were chosen.

At 300 K the higher energy crystal field components of the two multiples involved cannot be assumed empty and the spectra measured are envelopes of numerous spectral lines related to transitions between individual crystal field levels. When the temperature diminishes the populations of higher energy crystal field levels of initial multiplets become smaller. As a consequence the spectra at 80 K show more pronounced structure. Nevertheless, at 80 K the  $kT \sim 56$  cm<sup>-1</sup> and the Boltzmann statistics indicates that the population of the higher energy components of the ground multiplet <sup>4</sup>I<sub>15/2</sub> is close to 30% of total multiplet population and thereby absorption spectra recorded at 80 K remain still complex. Well defined absorption maxima at 1490.5, 1504.5, 1515 and 1520 nm are convenient for optical pumping. Their spectral widths are large enough to match typical bandwidth of laser diode emission of 2 nm. It is worth noticing that these four maxima are preponderant also in 5 K absorption spectra (shown in Fig. 3) indicating that they are related to transitions from the lowest energy crystal field levels of the ground state. Examination of the absorption bands in Fig. 4 reveals clearly that the overall band areas and the band structures diminish when the temperature increases from 80 to 300 K.

The middle panel in Fig. 4 shows the <sup>4</sup>I<sub>13/2</sub> → <sup>4</sup>I<sub>15/2</sub> emission spectra calibrated in units of stimulated-emission cross section  $\sigma_e$  using the Füchtbauer-Ladenburg (FL) relation [34]:

**Fig. 4** Absorption cross section spectra (upper), stimulated-emission cross section spectra (medium) at several different temperatures between 80 and 300 K and gain G spectra at 80 K (bottom) for 0.5at% Er:CaF<sub>2</sub> crystal



$$\sigma_e(\lambda) = \frac{\beta}{8\pi n^2 c \tau} \frac{\lambda^5 I(\lambda)}{\int \lambda I(\lambda) d\lambda} \tag{3}$$

where  $I(\lambda)/\int \lambda I(\lambda) d\lambda$  is a normalized lineshape function of the experimental emission spectrum  $I(\lambda)$ , luminescence branching ratio  $\beta = I$  for the  ${}^4I_{13/2} \rightarrow {}^4I_{15/2}$  Er<sup>3+</sup> transition,  $\tau$  is the  ${}^4I_{13/2}$  radiative lifetime,  $n$  is the refractive index and  $c$  is the velocity of light. To obtain spectra  $\sigma_e(\lambda)$  from Eq. (3) the radiative lifetime values  $\tau$  should be known. The  ${}^4I_{13/2} \rightarrow {}^4I_{15/2}$  transition obeys the selection rules  $\Delta L = 0$ ,  $\Delta S = 0$ ,  $\Delta J = 0, 1$  ( $0 \neq 0$ ). Hence, magnetic dipole transitions are allowed and the relaxation rate of the  ${}^4I_{13/2}$  excited state of Er<sup>3+</sup> is a sum of the electric dipole transition rate A(ED) and of the magnetic dipole transition rate A(MD). The inverse of the sum A(ED) + A(MD) is the  ${}^4I_{13/2}$  radiative lifetime  $\tau$ . Values of the oscillator strength P(MD) and corresponding rate A(MD) for magnetic dipole transition were calculated using relations given elsewhere [21]. The calculated P(MD) value was then subtracted from experimental oscillator strengths  $P_{exp}$  and eventually, electric dipole oscillator strengths P(ED) were obtained. Next, values of the A(ED) were determined inserting P(ED) to the relation [21]:

$$A(ED) = \frac{8\pi^2 e^2 n^2}{m c \lambda^2} \times \frac{2J' + 1}{2J + 1} \times P(ED) \tag{4}$$

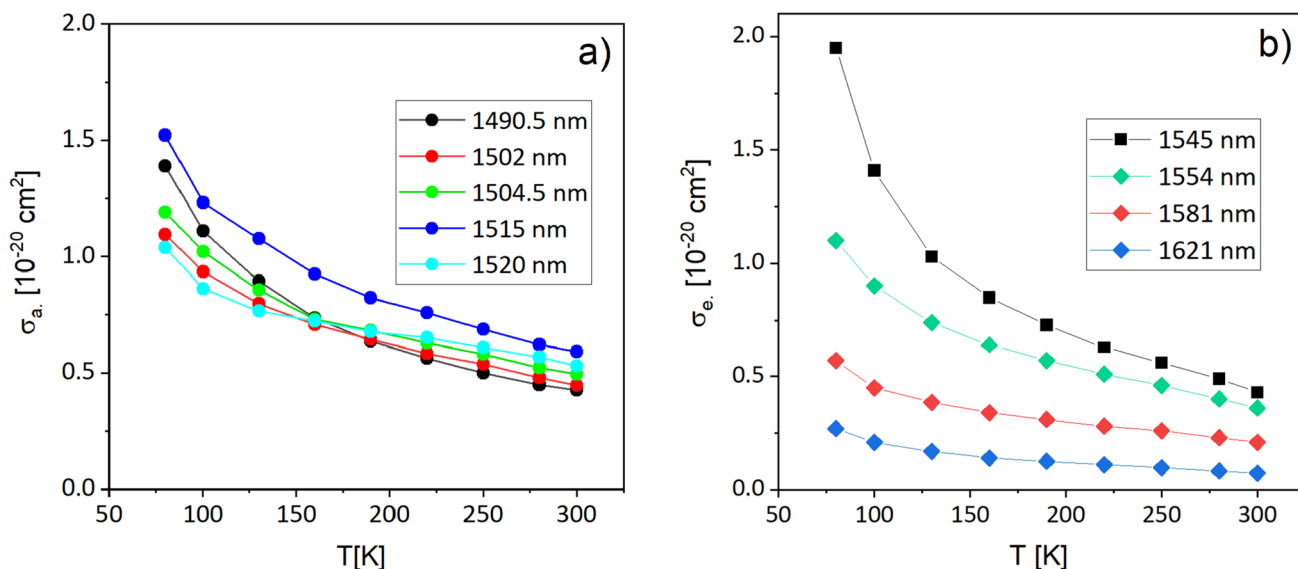
where  $n$  is the refractive index, the values of  $J'$  and  $J$  are 13/2 and 15/2 respectively,  $\lambda$  denotes emission wavelength,

symbols  $c$ ,  $m$  and  $e$  denote speed of light, electron mass and electron charge respectively.

Emission spectrum at 80 K shows well defined local maxima at 1545, 1554, 1581 and 1621 nm. When the temperature increases the overall emission band intensity diminishes and its structure is less complex.

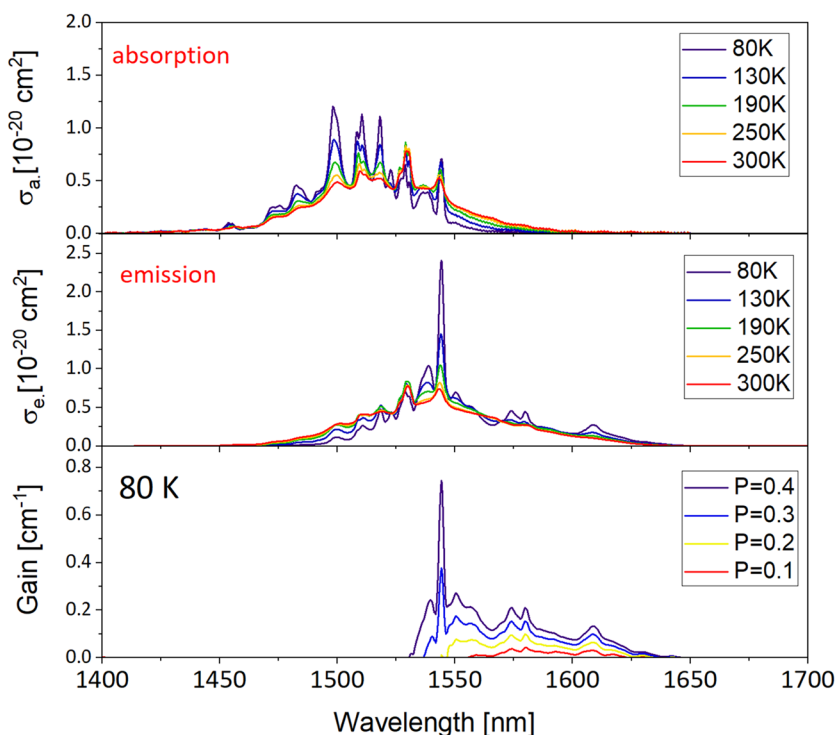
In Fig. 5 the values of absorption cross section and emission cross section at the wavelengths of local maxima mentioned above for Er<sup>3+</sup>:CaF<sub>2</sub> are plotted versus temperature in the region 80 K – 300 K. It can be seen that the local maximum at 1515 nm shows the highest absorption cross section for all wavelengths in this region. The change of temperature from 80 to 300 K brings about a decrease of its peak absorption cross section from  $1.52 \times 10^{-20} \text{ cm}^2$  to  $0.59 \times 10^{-20} \text{ cm}^2$ . For the same change of the temperature the peak absorption cross section at remaining wavelengths decreases by a factor of 2 roughly. The peak stimulated-emission cross section is the highest at 1545 nm. It attains  $1.95 \times 10^{-20} \text{ cm}^2$  at 80 K and  $0.43 \times 10^{-20} \text{ cm}^2$  at 300 K. Values of the peak stimulated-emission cross section at remaining wavelengths mentioned above are lower and their dependence on the temperature is rather moderate.

Figure 6 compares absorption spectra (upper) and emission spectra (medium) at several different temperatures between 80 and 300 K for Er<sup>3+</sup>:SrF<sub>2</sub> crystal. Five temperatures were chosen. Well defined absorption maxima at 1498, 1508.5, 1510.5 and 1518 nm are convenient for



**Fig. 5** Absorption cross section (a) and stimulated-emission cross section (b) at wavelengths of several local maxima for Er:CaF<sub>2</sub> plotted versus temperature in the region 80 K – 300 K

**Fig. 6** Absorption cross section spectra (upper), stimulated-emission cross section spectra (medium) at several different temperatures between 80 and 300 K and gain G spectra at 80 K (bottom) for 0.6at% Er:SrF<sub>2</sub> crystal



optical pumping. Their spectral widths are large enough to match typical bandwidth of laser diode emission of 2 nm. Four maxima given above are preponderant also in 5 K absorption spectra (shown in Fig. 3) indicating that they are related to transitions from the lowest energy crystal field levels of the ground state. Examination of absorption bands in Fig. 6 reveals clearly that the overall band

areas diminish and the band structures vanish when the temperature increases from 80 to 300 K.

The emission spectrum at 80 K shows well defined local maxima at 1544, 1574, 1580 and 1609 nm. When the temperature increases the overall emission band intensity diminishes and its structure becomes weaker.

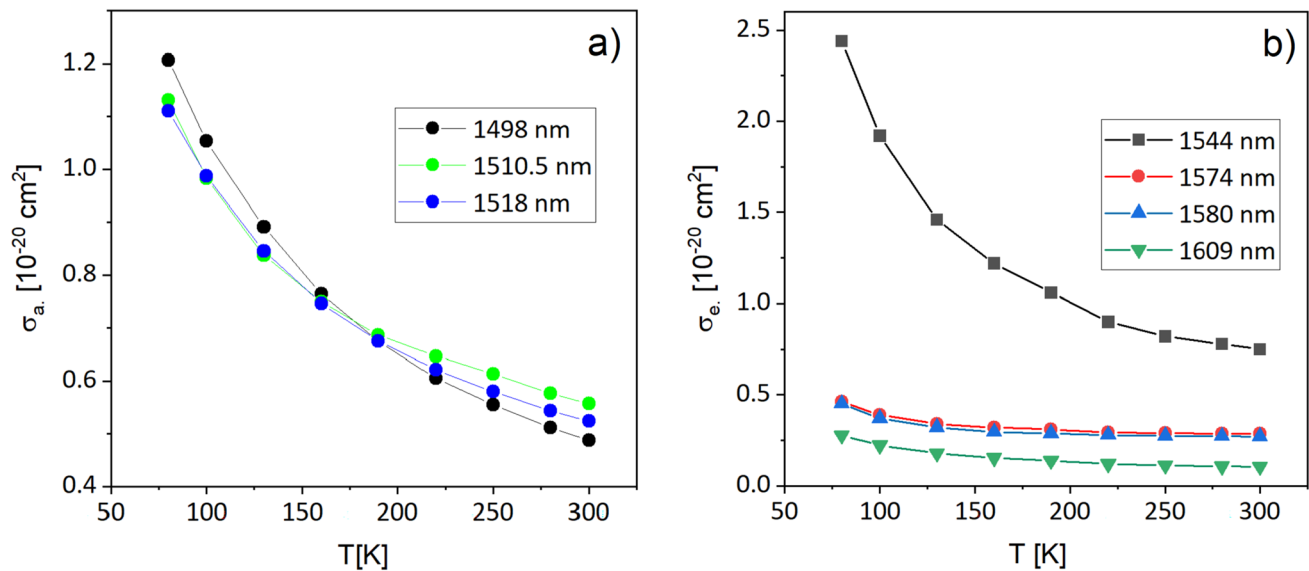


**Fig. 7** Absorption cross section (a) and stimulated-emission cross section (b) at wavelengths of several local maxima for Er:SrF<sub>2</sub> plotted versus temperature in the region 80 K – 300 K

In Fig. 7 the values of absorption cross section and stimulated-emission cross section at wavelengths of local maxima mentioned above for Er<sup>3+</sup>:SrF<sub>2</sub> are plotted versus temperature in the region 80 K – 300 K. It can be seen that the local maximum at 1498 nm shows the highest absorption cross section of about  $1.22 \times 10^{-20} \text{ cm}^2$  at 80 K but its decrease is steep and at 300 K it is the smallest amounting to  $0.49 \times 10^{-20} \text{ cm}^2$ . The values of absorption cross section for local maxima at remaining wavelengths are smaller and their dependence on the temperature is rather moderate. The peak emission cross section is the highest at 1544 nm. It attains  $2.44 \times 10^{-20} \text{ cm}^2$  at 80 K and  $0.75 \times 10^{-20} \text{ cm}^2$  at 300 K. The values of the peak stimulated-emission cross section at remaining wavelengths mentioned above are markedly lower and their dependence on the temperature is rather moderate.

Our stimulated-emission cross section data depend crucially on radiative lifetime values inserted to Eq. (3). Labbe et al. [4] have determined  $\tau = 7.7 \text{ ms}$  for the  $^4I_{13/2}$  level of Er<sup>3+</sup> in CaF<sub>2</sub>. This value was obtained from the Judd–Ofelt analysis of absorption spectra averaged over several Er<sup>3+</sup> concentrations between 0.49 at% and 10.34 at%. The J–O parameters then obtained are:  $\Omega_2 = 1.22$ ,  $\Omega_4 = 0.98$ ,  $\Omega_6 = 1.72$  (in units of  $10^{-20} \text{ cm}^2$ ). Kumar et al. [12] performed the Judd–Ofelt analysis of absorption spectra recorded for Er:CaF<sub>2</sub>. They obtained the J–O parameters:  $\Omega_2 = 6.6$ ,  $\Omega_4 = 2.3$ ,  $\Omega_6 = 2.0$  (in units of  $10^{-20} \text{ cm}^2$ ). These values are markedly higher than those reported by Labbe et al. but curiously they gave longer  $\tau = 8.4 \text{ ms}$ . In our approach  $\tau = 7.1 \text{ ms}$  at 300 K for Er:CaF<sub>2</sub> and  $\tau = 7.6$  at 300 K for Er:SrF<sub>2</sub> was determined employing Eq. (4), (fundamental formula of absorption spectroscopy) [35]. It can be seen that three  $\tau$

values for the  $^4I_{13/2}$  level of Er<sup>3+</sup> in CaF<sub>2</sub> mentioned above agree quite well. However in view of significant differences in the J–O parameters involved this agreement may be accidental. In our opinion the reliability of this parameter waits for the verification.

Actual emission cross-section values for the  $^4I_{13/2} \rightarrow ^4I_{15/2}$  transition will be smaller due to the adverse effect of self-absorption. Graphs included in the bottom of Figs. 4 and 6 show a plot of a gain coefficient  $G(\lambda)$  at 80 K for several small values of population inversion parameter  $P$  versus wavelength according to Eq. (2). It is worth noticing that S.A. Pollack in his pioneer work [1] observed a free running laser operation at 1617 nm at 77 K. Our emission and  $G(\lambda)$  spectra at 80 K shown in Fig. 4 are consistent with this report. It follows from Eq. (2) that in regions where  $\sigma_a$  may be neglected, i.e. at wavelengths longer than 1590 nm for Er:CaF<sub>2</sub> and 1600 nm for Er:SrF<sub>2</sub> the  $G(\lambda)$  values at 80 K and 300 K would be essentially the same. In fact, it can be seen in Figs. 4&6 that  $\sigma_e$  is affected weakly by the temperature and at 300 K it equals to  $\sim 0.07 \times 10^{-20} \text{ cm}^2$  at 1621 nm for CaF<sub>2</sub>:Er and to  $\sim 0.1 \times 10^{-20} \text{ cm}^2$  at 1609 nm for Er:SrF<sub>2</sub>. Even for the parameter  $P$  as small as 0.1 the corresponding  $G(\lambda)$  values are higher nearly by one order of magnitude than scatter losses encountered in laser crystals, typically  $\sim 0.001\text{--}0.002 \text{ cm}^{-1}$  [36]. The plots of  $G(\lambda)$  imply also that for higher  $P$  parameters the Er:CaF<sub>2</sub> and Er:SrF<sub>2</sub> lasers with a properly chosen dispersive element inserted in a laser cavity would be able to emit radiation tuned between about 1575 nm and 1620 nm. Significant advantage of resonantly pumped erbium lasers emitting near 1.6  $\mu\text{m}$  resides in that the difference between absorbed and emitted photon



energy, denoted as quantum defect (QD) is very small. In fact, in Er:CaF<sub>2</sub> laser emitting at 1621 nm, pumped at 1504.5 nm the QD = 480 cm<sup>-1</sup>, i.e. ~7% of absorbed pump energy that is converted to heat in a laser crystal. Similarly, in Er:SrF<sub>2</sub> laser emitting at 1609 nm, pumped at 1498 nm the QD = 461 cm<sup>-1</sup>, i.e. ~6.9% of absorbed pump energy that is converted to heat in a laser crystal. When pumping into absorption bands located at wavelengths closer to the wavelength of the 0–0 line the QD value would be markedly smaller.

## 4 Conclusions

Room temperature absorption spectra related to the <sup>4</sup>I<sub>15/2</sub> → <sup>4</sup>I<sub>13/2</sub> transition of Er<sup>3+</sup> ions in single crystal samples of CaF<sub>2</sub> containing 0.05, 0.1, 0.3, 0.5 at%Er<sup>3+</sup> were found to be similar with respect to the overall band width and the distribution of local maxima contained therein. The same conclusion concerns single crystal samples of SrF<sub>2</sub> containing 0.05, 0.1, 0.2, 0.6 at%Er<sup>3+</sup>. Spectra recorded for samples cooled down to 5 K were analyzed referring to published data of EPR [27], high resolution selective laser spectroscopy and far infrared absorption investigation indicating that preponderant optical centers consist of single Er<sup>3+</sup> ions in tetragonal, trigonal and cubic sites. Analysis of absorption and luminescence spectra recorded at several temperatures from 80 to 300 K provided an in-depth knowledge on effects of temperature on factors that govern the efficiency of resonant optical pumping and lasing ability of Er<sup>3+</sup> ions imbedded in CaF<sub>2</sub> and SrF<sub>2</sub> hosts. For instance, a local absorption maxima at 1515 nm and 1498 nm show the highest absorption cross section at all wavelengths in this region for Er:CaF<sub>2</sub> and Er:SrF<sub>2</sub>, respectively. The peak stimulated-emission cross section is the highest at 1545 nm for the two systems. It attains 1.95 × 10<sup>-20</sup> cm<sup>2</sup> at 80 K and 0.43 × 10<sup>-20</sup> cm<sup>2</sup> at 300 K for Er:CaF<sub>2</sub> and 2.44 × 10<sup>-20</sup> cm<sup>2</sup> at 80 K and 0.75 × 10<sup>-20</sup> cm<sup>2</sup> at 300 K for Er:SrF<sub>2</sub>. Quantum defect (QD) value for the two systems is below 10%.

**Acknowledgements** This work was supported by National Natural Science Foundation of China (61925508), Science and Technology Commission of Shanghai Municipality (20520750200), International Partnership Program of Chinese Academy of Sciences (121631KYSB20200039). B. Macalik, J. Komar, R. Kowalski, A. Strzep and W. Ryba-Romanowski acknowledge National Centre for Research and Development of Poland for a support under a project Contract No.WPC2/1/SCAPOL/2021.

**Author contributions** RL: Conceptualization, Investigation, Formal Analysis, Writing—original draft preparation. BM: Methodology, Investigation, Formal Analysis. JK: Methodology, Investigation. RK: Methodology, Investigation. AS: Methodology, Investigation, Funding Acquisition. ZZ: Methodology, Investigation. ZZ: Methodology, Investigation. YW: Methodology, Investigation. LS: Investigation, Project administration, Funding Acquisition, Writing—original draft

preparation. WR: Conceptualization, Formal Analysis, Project administration, Supervision, Writing—original draft preparation.

## Declarations

**Conflict of interest** The authors declare no competing interests.

**Open Access** This article is licensed under a Creative Commons Attribution 4.0 International License, which permits use, sharing, adaptation, distribution and reproduction in any medium or format, as long as you give appropriate credit to the original author(s) and the source, provide a link to the Creative Commons licence, and indicate if changes were made. The images or other third party material in this article are included in the article's Creative Commons licence, unless indicated otherwise in a credit line to the material. If material is not included in the article's Creative Commons licence and your intended use is not permitted by statutory regulation or exceeds the permitted use, you will need to obtain permission directly from the copyright holder. To view a copy of this licence, visit <http://creativecommons.org/licenses/by/4.0/>.

## References

1. S. A. Pollack, Stimulated emission in CaF<sub>2</sub>:Er<sup>3+</sup>. Proc. IEEE **51**, 1793–1974 (1963)
2. C. Wyss, W. Luthy, H.P. Weber, P. Rogin, J. Hulliger, Opt. Commun. **139**, 215 (1997)
3. M. Pollnau, W. Luthy, H.P. Weber, T. Jensen, G. Huber, A. Casanio, H.P. Jenssen, R.A. McFarlane, Opt. Lett. **21**, 48 (1996)
4. C. Labbe, J.L. Doualan, P. Camy, R. Moncorge, M. Thuau, The 2.8 μm laser properties of Er<sup>3+</sup> doped CaF<sub>2</sub> crystals. Opt. Commun. **209**, 193–199 (2002)
5. T.T. Basiev, Yu.V. Orlovskii, M.V. Polyachenkova, P.P. Fedorov, S.V. Kuznetsov, V.A. Konyushkin, V.V. Osiko, O.K. Alimov, A.Yu. Dergachev, Continuously tunable cw lasing near 2.75 μm in diode-pumped Er<sup>3+</sup>:SrF<sub>2</sub> and Er<sup>3+</sup>:CaF<sub>2</sub> crystals. Quantum Electron. **36**, 591–594 (2006)
6. J. Sulc, P. Nemeč, R. Sveikar, H. Jelinkova, M.E. Doroshenko, P.P. Fedorov, V.V. Osiko, Diode-pumped Er:CaF<sub>2</sub> ceramic 2.7 μm tunable laser. Opt. Lett. **38**, 3406–3409 (2013)
7. W. Ma, Su. Liangbi, Xu. Xiaodong, J. Wang, D. Jiang, L. Zheng, X. Fan, C. Li, J. Liu, Xu. Jun, Effect of erbium concentration on spectroscopic properties and 2.79 μm laser performance of Er:CaF<sub>2</sub> crystals. Opt. Mat. Express **6**, 409X – 4151 (2016)
8. W. Ma, Su. Liangbi, Xu. Xiaodong, J. Wang, D. Jiang, L. Zheng, J. Liu, X. Fan, J. Liu, Xu. Jun, Improved 2.79 μm continuous-wave laser performance from a diode-end pumped Er, Pr:CaF<sub>2</sub> crystal. J. Alloys Compds. **695**, 3370–3375 (2017)
9. M. Fan, T. Li, J. Zhao, S. Zhao, G. Li, K. Yang, Su. Liangbi, H. Ma, C. Kränkel, Continuous wave and ReS<sub>2</sub> passively Q-switched Er:SrF<sub>2</sub> laser at ~3 μm. Opt. Lett. **43**, 1726 (2018)
10. Zhen Zhang, Wu. Qinghui, Yangxiao Wang, Zhonghan Zhang, Jingya Wang, Jingjing Liu, Jie Liu, Su. Liangbi, Efficient 2.76 μm continuous-wave laser in extremely lightly Er-doped CaF<sub>2</sub> single-crystal fiber. Laser Phys. Lett. **17**, 085801 (2020)
11. Y. Wang, F. Ma, Z. Zhang, Y. Wang, Wu. Qinghui, J. Liu, J. Liu, Z. Chen, Su. Liangbi, Revisiting the self-termination effect of erbium based near 3 μm mid-infrared lasers. J. Lumin. **252**, 119339 (2022)
12. G.A. Kumar, R. Riman, S.C. Chae, Y.N. Yang, I.K. Bae, H.S. Moon, Synthesis and spectroscopic characterization of CaF<sub>2</sub>:Er<sup>3+</sup> single crystal for highly efficient 1.53 μm amplification. J. Appl. Phys. **95**, 3243–3249 (2004)

13. C. Labbe, J.L. Doualan, R. Moncorge, A. Braud, P. Camy, Excited state absorption and fluorescence dynamics in Er:CaF<sub>2</sub>. *J. Lumin.* **200**, 74–80 (2018)
14. R. Sveikar, J. Sulc, M. Nemeč, H. Jelinkova, M.E. Doroshenko, V.A. Konyushkin, A.N. Nakkladov, V.V. Osiko, Effect of cryogenic temperature on spectroscopic and laser properties of Er, La:SrF<sub>2</sub>-CaF<sub>2</sub> crystal. *Proc. SPIE* **9726**, 97261C-1-97261C-7 (2015)
15. N. Ter-Gabrielyan, V. Fromzel, L.D. Merkle, M. Dubinskii, Resonant in-band pumping of cryo-cooled Er<sup>3+</sup>:YAG laser at 1532, 1534 and 1546 nm: a comparative study. *Opt. Mat. Express* **1**, 223–233 (2011)
16. M. Němec, P. Boháček, R. Švejkar, J. Šulc, J. Kratochvíl, H. Jelínková, B. Trunda, L. Havlák, M. Nikl, K. Jurek, Tunable resonantly pumped Er:GGAG laser. *Laser Phys.* **32**, 015802 (2022)
17. N. Ter-Gabrielyan, V. Fromzel, W. Ryba-Romanowski, T. Lukaszewicz, M. Dubinskii, Spectroscopic and laser properties of resonantly (in-band) pumped Er:YVO<sub>4</sub> and Er:GdVO<sub>4</sub> crystals: a comparative study. *Opt. Mat. Express* **2**, 1040 (2012)
18. Xu Chonglei, A. Strzep, Z. Zhang, H. Kou, Fengkai Ma Liangbi Su Growth and spectroscopic properties of Ca<sub>x</sub>Sr<sub>1-x</sub>F<sub>2</sub>: Sm: Gd single crystals. *J. Lumin.* **249**, 119008 (2022)
19. J.P. Russel, The Raman spectrum of calcium fluoride. *Proc. Roy. Soc.* **85**, 194–197 (1965)
20. A.V. Warriar, R.S. Krishnan, Raman spectrum of SrF<sub>2</sub>. *Die Naturwissenschaften* **51**, 8–9 (1964)
21. R. Reisfeld, Optical properties of lanthanides in condensed phase, theory and applications. *AIMS Mater. Sci.* **2**, 37–60 (2015)
22. N.J. Cockroft, D. Thompson, G.D. Jones, R.W.G. Syme, Site selective spectroscopy of hydrogenic sites in CaF<sub>2</sub>:Er<sup>3+</sup> crystals. *J. Phys. Chem.* **86**, 521 (1987)
23. N.J. Cockroft, G.D. Jones, R.W.G. Syme, Site-selective laser spectroscopy of deuterated SrF<sub>2</sub>:Er<sup>3+</sup> crystals. *J. Chem. Phys.* **92**, 2166 (1990)
24. E. Vinogradova, L. Dolgov, V.A. Konyushkin, E.O. Orlovskaya, E.A. Vagapova, A. Treshchalov, V. Peet, V. Hizhnyakov, Yu. V. Orlovskii, Fluorescence of Nd<sup>3+</sup> optical centers close to cubic symmetry in a calcium fluoride crystal co-doped with Na<sup>+</sup>. *J. Lumin.* **234**, 117988 (2021)
25. D.R. Tallant, J.C. Wright, Selective laser excitation of charge compensated sites in CaF<sub>2</sub>:Er<sup>3+</sup>. *J. Chem. Phys.* **63**, 2074–2085 (1975)
26. M.R. Brown, K.G. Roots, J.M. Williams, W.A. Shand, C. Groter, H.F. Kay, Experiments on Er<sup>3+</sup> in SrF<sub>2</sub>. II. Concentration dependence of site symmetry. *J. Chem. Phys.* **50**, 891–899 (1969)
27. C.W. Rector, B.C. Pandey, H.W. Moos, *J. Chem. Phys.* **45**, 171–179 (1966)
28. J.-P.R. Wells, T. Dean, R.J. Reeves, Site selective spectroscopy of the C<sub>3v</sub> symmetry center in Er<sup>3+</sup> doped BaF<sub>2</sub>. *J. Lumin.* **96**, 239–248 (2002)
29. J.-P.R. Wells, R.J. Reeves, Polarized laser-selective excitation and Zeeman infrared absorption of Sm<sup>3+</sup> in CaF<sub>2</sub> and SrF<sub>2</sub> crystals. *Phys. Rev. B* **61**, 13593–13608 (2000)
30. B. Jeżowska-Trzebiatowska, W. Ryba-Romanowski, Z. Mazurak, J. Hanuza, Investigations of the vibronic transitions in Cs<sub>2</sub>NaErCl<sub>6</sub>. *Chem. Phys.* **50**, 209–216 (1980)
31. W. Ryba-Romanowski, Z. Mazurak, B. Jeżowska-Trzebiatowska, Investigation of emission spectra and lifetimes of Cs<sub>2</sub>NaErCl<sub>6</sub> single crystals. *J. Lumin.* **27**, 177–189 (1981)
32. J.P. Aubry, G. Morlot, G. Villermain-Lecolier, A. Hadni, Far infrared spectra of strontium fluoride doped with rare earth. *Infrared Phys.* **18**, 901–908 (1978)
33. D.C. Brown, N.S. Tomasello, C.L. Hancock, Absorption and emission cross-sections, Stark energy levels, and temperature dependent gain of Yb:QX phosphate glass. *Opt. Express.* **29**, 33818 (2021)
34. B. Aull, H. Jenssen, Vibronic interactions in Nd:YAG resulting in nonreciprocity of absorption and stimulated emission cross sections. *IEEE J. Quantum Electron.* **18**, 925 (1982)
35. B. Di Bartolo, *Optical interactions in solids* (John Wiley & Sons, New York-London-Sydney-Toronto, 1968)
36. W. Koechner, *Solid state laser engineering* (Springer-Verlag, New York, Heidelberg, Berlin, 1976)

**Publisher's Note** Springer Nature remains neutral with regard to jurisdictional claims in published maps and institutional affiliations.